Power Decoupling Strategy of QAB Converters for DC Microgrids with Islanding Operations

Chang-Woo Yun[1], Jun-Suk Lee[2], Kyung-Wook Heo[2], and Jee-Hoon Jung[2]
[1] Hyundai Motors, South Korea
[2] Electrical Engineering, Ulsan National Institute of Science and Technology, South Korea

***Abstract* - Multiport DC-DC converters based on a dual-active-bridge (DAB) structure have attracted attention due to their high-power density and bidirectional power transfer in DC microgrid systems. Reliability is also high in connecting to various distributed resources (DRs). However, power coupling among ports magnetically connected by a single transformer induces poor power control and voltage regulation performance. To solve those problems, an enhanced power decoupling method for a quadraple-active-bridge (QAB) converter is proposed, which does not have supplementary decoupling components and control algorithms under both grid-connected and islanding mode operations of the DC microgrid system. In addition, a modular structure can be applied to individually connect with various loads. Finally, a 3-kW prototype QAB converter is implemented to verify the validity and performance of the proposed method.**

***Index Terms*-- QAB Converter, Power Decoupling, DC Microgrid, Islanding Operation.**

I. Introduction

Since DC microgrids have various advantages over AC systems, a lot of interest and research have been conducted. The AC system, which has been used for decades, has already been built in infrastructure and can be used without additional facilities. However, an AC-DC converter is required to connect to DC loads, and power loss occurs because of the skin effect caused by AC power. In addition, synchronized operation and reactive power problems can occur. Instead of using the AC system, recently a DC microgrid including renewable energy and energy storage system (ESS) is attracting attention for specific applications such as smart buildings and data centers.

The DC system shown in Fig. 1 has advantages such as no synchronization problem, no reactive power loss, and no AC-DC power converters. The DC system has high reliability because it can operate a grid independently by connecting it to various distributed resources (DRs) such as ESS and PV [1]. The DC microgrid has two operating modes: Grid-connected mode and Islanding mode depending on the operating state of the power grid [2]. The grid-connected mode directly supplies power from grids to loads; however, the islanding mode continuously supplies power from the DR or the ESS to loads without interruption under grid fault situations such as black-out and short and open circuits. The charging and discharging of the DRs are determined by the operating condition of the grid system, therefore, the operating modes have high flexibility. In the DC microgrid system, a dual-active-bridge (DAB) converter is widely used to obtain the capabilities of bidirectional power flow control, galvanic isolation, and soft switching. Both input and output ports are composed of two bridge legs, and power is transferred by using the phase difference of each port. The magnitude and direction of the transferred power are determined by the phase difference called phase-shift control [3]-[4].

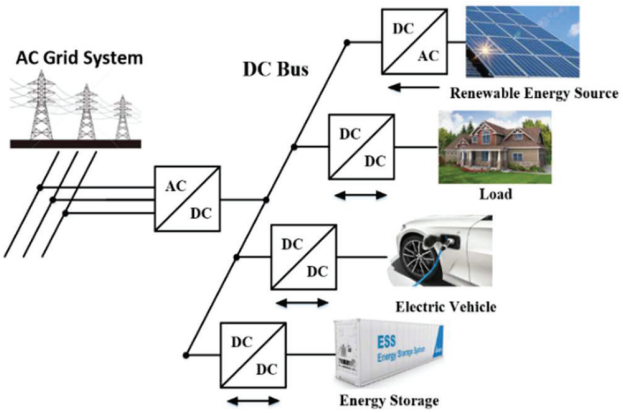

Fig. 1. Conceptual schematic of the DC microgrid.

In Fig. 2, a multiport DAB converter has high power density, high conversion efficiency, and fast dynamic response compared with a single DAB converter. However, conventional multiport converters have power coupling issues among arbitrary output ports due to a multi-winding transformer. The power coupling is an unintended effect, which decreases the dynamic performance of the converter and makes it difficult to tightly regulate the output voltage.

For the multiport DAB converter, various power decoupling methods have been proposed to solve those problems. To minimize the power coupling phenomenon, transformer modeling and optimal winding methods have been proposed in the early design stage; however, it is difficult to keep the performance improvement for various applications [10], [11]. The power decoupling algorithm using look-up table (LUT) values is proposed, which compensates for power fluctuations in advance at each decoupling point. However, its computation burden and control complexity are significant [12]. A compensating method of power coupling using a resonant tank has been proposed [13]. It has a drawback due to the inability to

This work was supported by the Korea Institute of Energy Technology Evaluation and Planning (KETEP), funded by the Korea Government (MOTIE) under Grant 2022202090010B, for the development and demonstration of a control equipment technology for industry.

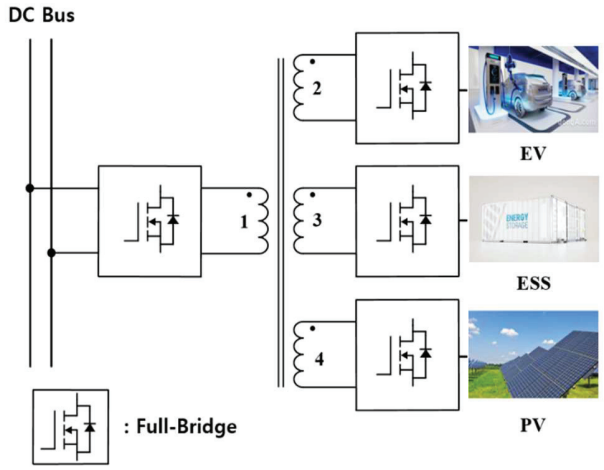

Fig. 2. Conceptual schematic of the multiport DAB converter.

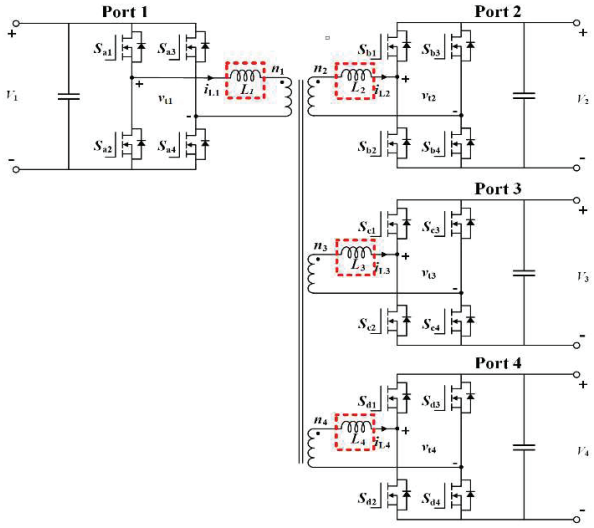

Fig. 3. Circuit diagram of the conventional multiport converter.

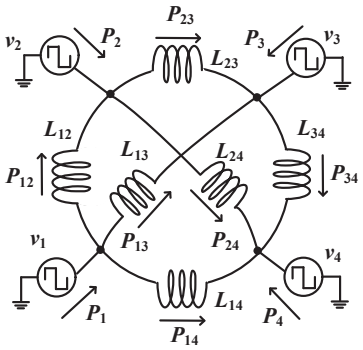

Fig. 4. Equivalent circuit and power flow of the conventional multiport converter.

bidirectional power transfer and the increment of conduction loss. Since achieving the power decoupling by removing the inductor of the input port cannot be applied to the islanding mode operations of the microgrid, its reliability becomes poor [14]-[16].

In this paper, the power decoupling strategy of a quadraple-active-bridge (QAB) converter is proposed by employing power decoupling capability under both the grid-connected mode and the islanding mode operations of the DC microgrid. The proposed topology can obtain the power decoupling capability using a selective coupling inductor combined with a relay circuit. It has no circuilating current and conduction loss in the input port inductor compared with the conventional multiport converter. Moreover, a modular structure can also be applied to individually connect with various loads. Finally, a 3-kW prototype QAB converter is implemented to experimentally verify the performance improvements of the proposed method.

II. Power Decoupling of Multiport Converters

Power coupling phenomena have been issued in the applications of multiport converters. In this section, the analysis of the power coupling phenomena and conventional power decoupling methods are discussed.

A. Power Coupling in Multiport Converters

A multiport-based QAB converter with four coupling inductors of L_1, L_2, L_3 and L_4 is illustrated in Fig. 3. A single core contains several windings that are shared in a conventional QAB converter and are magnetically connected to all other windings. An equivalent circuit and power flows are shown in Fig. 4. The ports are all connected by windings, and power coupling phenomena happen when the equivalent inductance of the output port alters the power flows, as shown in (1).

$$L_{ij} = L_i L_j \sum_{1}^{N=4} \frac{1}{L_N}, \forall i, j \in [1,4] \tag{1}$$

The power flows of P_{ij} are determined by the equivalent inductance and the phase shift angle of $\emptyset_{ij}$ as shown in (2).

$$P_{ij} = \frac{nV_{porti}V_{portj}\phi_{ij}(\pi - \phi_{ij})}{2\pi^2 f_{sw} L_{ij}}, \forall i, j \in [1,4] \tag{2}$$

The following is an expression for the power flow equations for each port, which include the power coupling phenomenon.

$$P_i = \begin{cases} P_{12} + P_{13} + P_{14}, & i = 1 \\ -P_{12} + P_{23} + P_{24}, & i = 2 \\ -P_{13} - P_{23} + P_{34}, & i = 3 \\ -P_{14} - P_{24} - P_{34}, & i = 4 \end{cases} \tag{3}$$

Changes in load in ot her ports have an impact on the power coupling phenomena. It reduces the dynamic

response of the converter system and makes it challenging to regulate the voltage of the output port by causing unwanted power changes in the port unrelated to the power flows.

B. Power Decoupling Methods

Several power decoupling methods are introduced in the chapter before [10]-[13]. However, one of the practical and easy ways to achieve power decoupling is to remove the input port inductance [14]-[16]. The equivalent inductances between the output ports become infinite by subtracting the coupling inductance of the input port (L_1), as follows:

$$L_{ij} = \begin{cases} L_j,\ i = 1, \forall j \in [2,4] \\ \dfrac{K}{L_1 L_j}, i \neq 1, \forall j \in [2,4] \\ \mathrm{K} = L_1L_2L_3 + L_1L_2L_4 + L_1L_3L_4 + L_2L_3L_4 \end{cases} \quad (4)$$

Except the input port inductor (L_1), this method employs the system's three output port inductors (L_2, L_3, L_4). High power density, efficiency, and reactive power that is not produced by the inductor at the input port have benefits [17]. However, this method can only be applied to the grid-connected mode. If the system operates at the islanding mode due to the occurrence of a fault situation, the DR port changes to the input port, so the power coupling phenomenon occurs with the inductor (L_4) of the DR port as follows:

$$P_{coupling} = \begin{cases} P_{23} + P_{24} + P_{34} & (Grid-connected\ mode) \\ P_{23} & (Islanding\ mode) \end{cases} \quad (5)$$

III. Proposed Multiport Converter

The proposed QAB converter's circuit diagram is shown in Fig. 5. It consists of four full-bridge converters, two relay circuits, and four coupling inductors. The input port inductor (L_1) is utilized to prevent transformer saturation in the islanding mode, while the three outport inductors (L_2, L_3, L_4) are used to transfer power across ports. The relay circuits are connected in parallel to the inductor of the input port and the DR port for selectively using both the grid-connected mode and the islanding mode. Furthermore, the proposed circuit can be applied to modular design using multiple single transformers instead of a multi-winding transformer. The advantages of this topology with the multiple single transformers have load scalability and simplicity of load change.

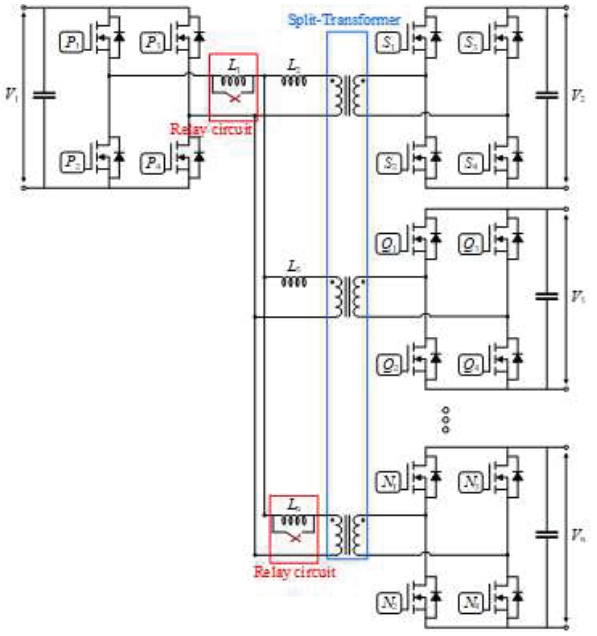

Fig. 5. Circuit diagram of the proposed multiport-based QAB converter.

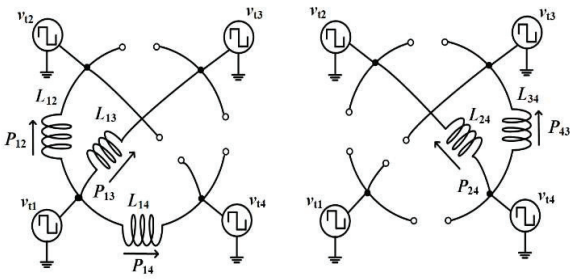

Fig. 6. Equivalent circuits of grid-connected and islanding modes.

Fig. 6 shows the equivalent circuit and power flows of the proposed converter. All of the output port's equivalent circuits are opened. Without any coupling power, the transferred power in the grid-connected mode (P_{12}, P_{13}, P_{14}) and islanding mode (P_{42}, P_{43}) can be represented as follows:

$$P = \begin{cases} P_{12} + P_{13} + P_{14}\ (Grid-conneceted\ mode) \\ P_{42} + P_{43} \qquad\qquad (Islanding\ mode) \end{cases} \quad (6)$$

In addition, the transferred power equations can be expressed in both the grid-connected mode as (7) and the islanding mode (8).

$$P_{ij} = \left(\frac{nV_{porti}V_{portj}\phi_{ij}(\pi - \phi_{ij})}{2\pi^2 f_{sw} L_{ij}},\ i = 1, \forall j \in [2,4] \right. \quad (7)$$

$$P_{ij} = \left(\frac{nV_{porti}V_{portj}\phi_{ij}(\pi - \phi_{ij})}{2\pi^2 f_{sw} L_{ij}},\ i = 4, \forall j \in [2,3] \right. \quad (8)$$

A. Relay Circuit

In order to choose whether to activate or deactivate the inductor depending on the operating mode, Fig. 7 shows a parallel connected circuit of an inductor and a relay. Current flows to the relay in the parallel circuit with a negligibly low impedance. The inductance disappears when the relay circuit is activated. On the other hand, when the relay circuit is deactivated, the inductance appears. In the grid-connected mode, the inductance of the input port (L_1) is deactivated, and the inductance of the DR port (L_4) is activated. In the islanding mode, the inductance of the input port (L_1) is activated, and the inductance of the DR port (L_4) is deactivated. Port inductances according to operating modes are shown in Table I. By achieving power decoupling in both the grid-connected and islanding modes, based on the proposed circuit for the multiport converter, the stability of the grid system can be increased. Since the relay circuit used in the proposed converter is a mechanical switch, it prevents resonance between the inductance and parasitic capacitance. Moreover, the mode transition only works when a fault condition occurs in the grid system. Therefore, the expected life of the relay circuit does not seem to be much considered.

B. Switching Algorithm

Open, shorts, blackout, and other fault situations are possible in the DC microgrid [18]. At that time, the grid system is unable to supply normal DC voltage, which can cause the malfunction of the converter and affect the loads. A switching algorithm presented in Fig. 8-(a) entirely blocks the input ports to prevent a converter system failure under fault conditions. It shows the switching algorithm at the input port. Depending on the fault condition, port 1 operates either upper switches on and lower switches off or upper switches off and lower switches on. As a result, the proposed multiport converter can normally operate in the islanding mode to be disconnected from the grid, regardless of the fault situations that occur in the grid system. Fig. 8-(b) shows an equivalent circuit diagram when the fault condition occurs and the proposed switching algorithm is conducted. The inductance of the input port (L_1) is used to prevent transformer saturation from fault conditions. Without L_1, the transformer is shorted to the node consisting of a switch S_2, S_4 turned on and S_1, S_3 turned off in port 1. During islanding mode, power cannot generally be transferred from the DR port to the load port.

Fig.9 shows a relay control algorithm at the mode tran sition. In order to provide power decoupling in both grid-connected and islanding modes, the relay circuit's operation is set differently. Depending on the fault

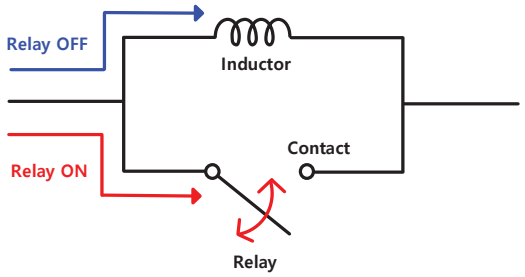

Fig. 7. Relay circuit connected to the inductor in parallel.

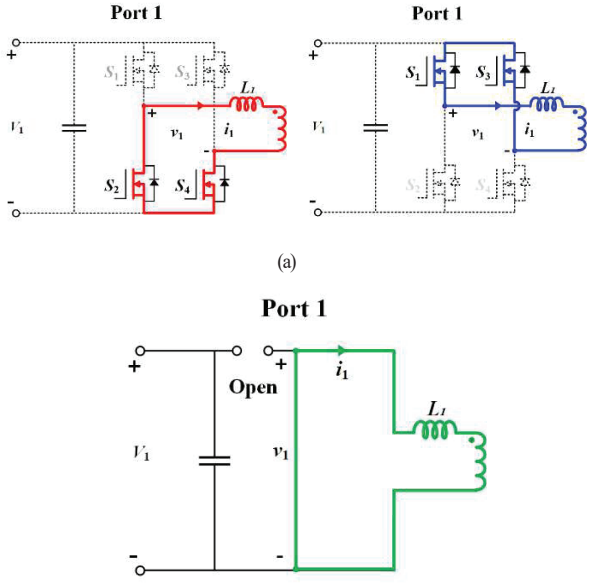

(a)

(b)

Fig. 8. Circuit diagram of the proposed switching algorithm under fault conditions at Port 1: (a) Switching algorithm with an inductor, (b) Equivalent circuit diagram

TABLE I
PORT INDUCTANCES IN ACCORDANCE WITH MODES

	Port1	Port2	Port3	Port4
Grid Connected Mode	*0*	L_2	L_3	L_4
Islanding Mode	L_1	L_2	L_3	*0*

situations, the operating mode is modified according to the state of the input port voltage (V_{in}). The mode is changed based on *360V*. A voltage below *360V* is regarded as very low voltage and unsafe status due to fault situations based on the *380V* rated voltage [19].

IV. Experimental Results

A 3-kW prototype is carried out to verify the power decoupling of the proposed converter. The prototype is shown in Fig. 10. Experiments using the prototype verify the dynamic performance and power decoupling

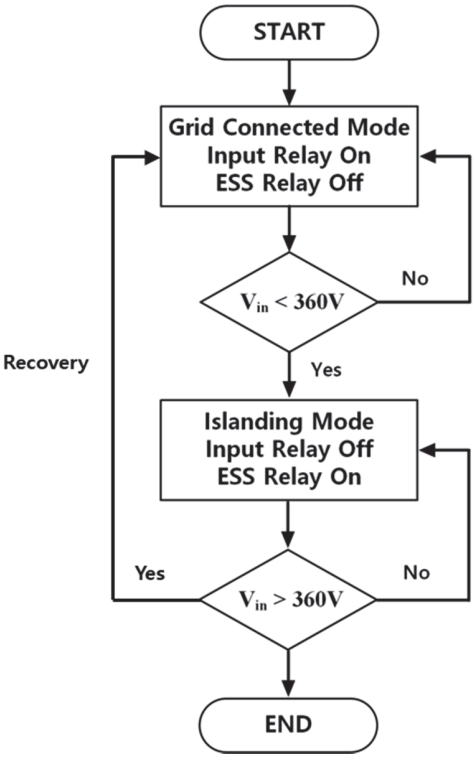

Fig. 9. Relay control algorithm at the mode transition

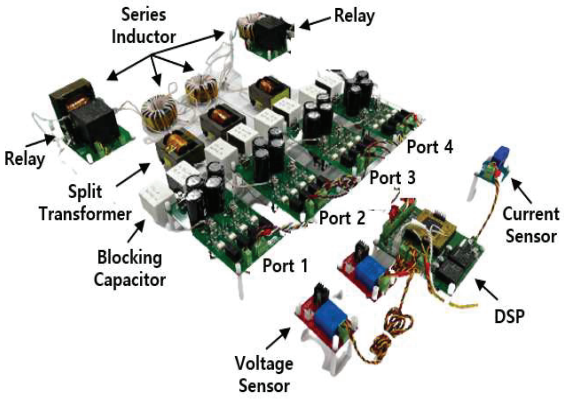

Fig. 10. Prototype of the proposed multiport QAB converter.

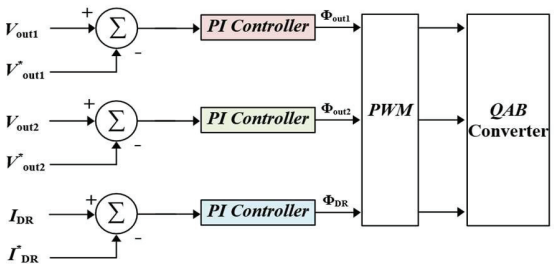

Fig. 11. Simplified block diagram of the closed-loop control system

performance when the step load is applied. The converter consists of four full-bridges, four coupling inductors, two relays, and three transformers. The experimental specifications of the parameters are shown in Table II. In addition, the devices used in the proposed converter are shown in Table III.

In the DR port, high current-rated MOSFETs are used by considering the current change during mode transition. In addition, DC-blocking capacitors are used for each port to prevent transformer saturation that occurs during mode transition. The magnitude of the coupling inductors is designed with a 30% margin based on a 1 kW power rating for each port. The inductance at port 1 to prevent the transformer saturation in the islanding mode is used in the same size as the magnetizing inductance of the transformer.

Fig. 11 shows a simplified closed-loop control system for each port of the proposed converter. Output loads are regulated by using proportional and integral (PI) controllers to manage $\emptyset_{out1}, \emptyset_{out2}$ and $\emptyset_{DR}$, which are the phase shifts of three outputs. Load variations are sensed using two voltage sensors (V_{out1}, V_{out2}) and a current sensor (I_{DR}), then a PI controller independently regulates the output voltage according to the load variations.

Fig. 12 shows the steady-state operating waveforms of the inductor voltage ($V_{L1}, V_{L2}, V_{L3}, V_{L4}$) and current ($I_{L1}, I_{L2}, I_{L3}, I_{L4}$) in the grid-connected mode and the

TABLE II
EXPERIMENTAL SPECIFICATIONS OF THE PROTOTYPE CONVERTER

Parameter	Value	Parameter	Value
V_{in}	380V	$L_{coupling}$	259uH 256uH
V_{out1}	380V	L_{relay}	3mH 255uH
V_{out2}	300V	***Turn Raito***	24:24:18:11
V_{DR}	180V	f_{sw}	50kHz
P_{out}	3kW	C_{block}	3uF

TABLE III
DEVICES USED IN THE PROPOSED CONVERTER

Device	Name
MOSFET (Bridge)	STW48N60M2
MOSFET (DR port)	IPW65R041
Relay	G9KA-1A
Microcontroller	TMS320F28335

islanding mode to verify the normal operation of the proposed converter.

Fig. 13 shows the step-load response where P_{out1} changes from 0.5 kW to 1 kW while V_{out2}keeps the constant voltage to approximately 300 V at the islanding mode except for the power distortion of 2.5 V (0.8 %

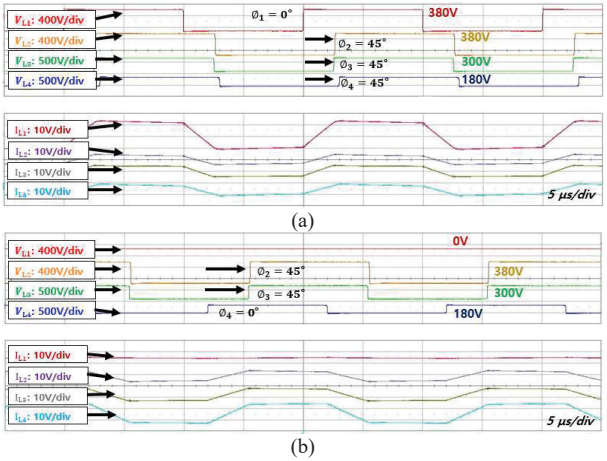

Fig. 12. Steady-state operating waveforms according to various load conditions: (a) Grid-connected mode, (b) Islanding mode.

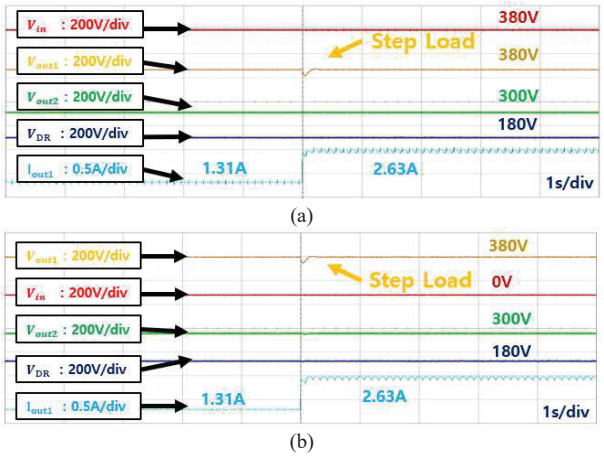

Fig. 13. Voltage waveforms according to step-load response (from 0.5 kW to 1 kW): (a) Grid-connected mode, (b) Islanding mode.

undershoot voltage) caused by the leakage inductance of the transformer. V_{out1} drop with 30 V (7.8 % undershoot voltage) with 0.25 ms settling time under the step load changes at port 1. Based on the experimental results, the power coupling phenomenon does not occur in both the grid-connected mode and the islanding mode by using the proposed power decoupling method.

Fig. 14 shows the experimental waveforms of mode transitions between the grid-connected mode and the islanding mode under the fault situation. In the grid-connected mode, V_{L1} of port 1 is supplied normally and I_{DR} of the DR port is charged by $6.2\ A$. However, as the fault situation occurred in the grid system, V_{L1} of port 1 becomes $0\ V$, and the operating mode changes to the islanding mode. The DR port is discharged by the current of $-13.2\ A$ supplied from the ESS battery and operates as an input port. If the grid system normally operates during the islanding mode, the operating mode is recovered to the grid-connected mode and I_{DR} of the DR port is charged by $6.2\ A$ again.

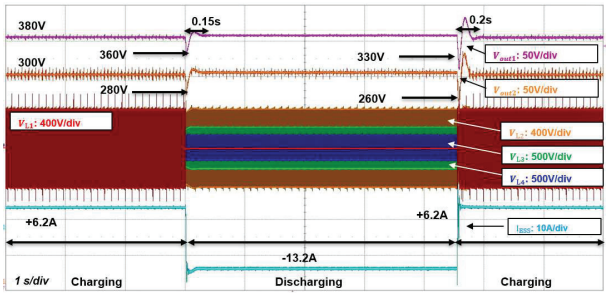

Fig. 14. Experimental waveforms of mode transitions.

V. Conclusions

The proposed QAB converter is presented in this paper and uses power decoupling capability in both the grid-connected mode and the islanding mode. By using the inductor and relay circuit, power decoupling is selectively conducted without the use of additional power decoupling algorithms. The modular structure is also used to connect alternative loads. A 3-kW prototype is used to experimentally verify the proposed converter. Step load response is verified that one output port changes from 0.5 kW to 1 kW, and the power decoupling performance can be obtained except for 0.8 % power distortion caused by the leakage inductance of the transformer. The proposed multiport converter has a grid-connected mode power conversion efficiency of up to 95.7% and an islanding mode power conversion efficiency of up to 94.7%. Depending on the operating mode, the switching algorithm and relay operation of the converter carries out the process of switching from the grid-connected mode to the islanding mode to transfer power continuously. In conclusion, by skipping the coupling inductor, the proposed converter reduces circulating power and conduction loss when used with the DC microgrid system. Also, the proposed power decoupling strategy enhances the stability of the multiport converter.

References

[1] D. Habumugisha, S. Chowdhury and S. P. Chowdhury, "A DC-DC interleaved forward converter to step - up DC voltage for DC Microgrid applications," 2013 IEEE Power & Energy Society General Meeting, 2013, pp. 1-5, doi: 10.1109/PESMG.2013.6672501.

[2] L. E. Zubieta, "Are Microgrids the Future of Energy?: DC Microgrids from Concept to Demonstration to Deployment," in IEEE Electrification Magazine, vol. 4, no. 2, pp. 37-44, June 2016, doi: 10.1109/MELE.2016.2544238.

[3] M. Pham, V. Hoang and H. Lee, "Cost effective synchronization strategy for distributed generators in islanded microgrids," Journal of Power Electronics, vol. 21, no. 3, pp. 583-589, 2021. DOI: 10.1007/s43236-020-00199-0.

[4] Zhang, L., Dai, L. & Zhao, C. Decentralized control strategy for storage systems in islanded microgrids. J. Power Electron. 21, 1834–1844 (2021). https://doi.org/10.1007/s43236-021-00315-8

[5] H. J. Choi and J. H. Jung, “Practical design of dual active bridge converter as isolated bi-directional power interface for solid state transformer applications,” J. Electr. Eng. Tech., Vol. 11, No. 5, pp. 1266-1273, Sep. 2016.

[6] D. Jeong, M. Ryu, H. Kim and H. Kim, "Optimized Design of Bi-Directional Dual Active Bridge Converter for Low-Voltage Battery Charger," Journal of Power Electronics, vol.14, no. 3, pp. 468-477, 2014. DOI:10.6113/JPE .2014.14 .3.468.

[7] H. Wen and B. Su, "Reactive Power and Soft-Switching Capability Analysis of Dual-Active-Bridge DC-DC Converters with Dual-Phase-Shift Control," Journal of Power Electronics, vol. 15, no. 1, pp. 18-30, 2015. DOI:10 .6113/JPE.2015.15.1.18.

[8] X. Sun, Z. Wang, Q. Zhang and G. Chen, "Variable frequency triple-phase-shift modulation strategy for minimizing RMS current in dual-active-bridge DC-DC converters," Journal of Power Electronics, vol. 21, no. 2, pp. 296-307, 2021. DOI: 10.1007/s43236-020-00183-8.

[9] Lee, S.H., Kim, B.K. & Kim, S. Single pulse width modulation for dual-active-bridge converters considering parasitic capacitance of MOSFETs. J. Power Electron. (2022). https://doi.org/10.1007/s43236-022-00544-5

[10] Diao, G. Zhu, A. Rockhill, H. Cao, Y. Wu and Y. Zhao, "Physics-Based Magnetic Modeling of a Three-Port Transformer in a Triple-Active-Bridge Converter with Decoupled Power Flow Regulation," 2022 IEEE Applied Power Electronics Conference and Exposition (APEC), 2022, pp. 1492-1499, doi:10.1109/APEC43599.2022.9773545.

[11] H. Beiranvand, F. Hoffmann, Y. Pascal, F. Hahn and M. Liserre, "Multiwinding Transformer Leakage Inductance Optimization for Power Flow Decoupling in Multiport DC-DC Converters," 2021 IEEE 15th International Conference on Compatibility, Power Electronics and Power Engineering (CPE-POWERENG), 2021, pp. 1-8, doi: 10.1109/CPE-POWERENG50821.2021.9501085.

[12] C. Zhao, S. D. Round and J. W. Kolar, "An Isolated Three-Port Bidirectional DC-DC Converter With Decoupled Power Flow Management," in IEEE Transactions on Power Electronics, vol. 23, no. 5, pp. 2443-2453, Sept. 2008, doi: 10.1109/TPEL.2008.2002056.

[13] P. Wang, X. Lu, W. Wang and D. Xu, "Hardware Decoupling and Autonomous Control of Series-Resonance-Based Three-Port Converters in DC Microgrids," in IEEE Transactions on Industry Applications, vol. 55, no. 4, pp. 3901-3914, July-Aug. 2019, doi:10.1109/TIA.2019.2906112.

[14] S. Bandyopadhyay, P. Purgat, Z. Qin and P. Bauer, "A Multiactive Bridge Converter With Inherently Decoupled Power Flows," in IEEE Transactions on Power Electronics, vol. 36, no. 2, pp. 2231-2245, Feb. 2021, doi:10.1109/TPEL .2020.3006266.

[15] J. Sim, J. Lee and J. Jung, "Isolated three-port DC-DC converter employing ESS to obtain voltage balancing capability for bipolar LVDC distribution system," Journal of Power Electronics, vol. 20, no. 3, pp. 802-810, 2020. DOI: 10.1007/s43236-020-00065-z.

[16] Liu, R., Xu, L., Kang, Y., Hui, Y. and Li, Y. (2018), Decoupled TAB converter with energy storage system for HVDC power system of more electric aircraft. The Journal of Engineering, 2018: 593-602.https://doi.org/10.1049/joe.2018.0033

[17] H. Bai and C. Mi, "Eliminate Reactive Power and Increase System Efficiency of Isolated Bidirectional Dual-Active-Bridge DC–DC Converters Using Novel Dual-Phase-Shift Control," in IEEE Transactions on Power Electronics, vol. 23, no. 6, pp. 2905-2914, Nov. 2008.

[18] Han, G., Liu, W., Lu, Z. et al. Fault-tolerant converter and fault-tolerant methods for switched reluctance generators. J. Power Electron. 22, 17231734(2022).https://doi.org/10.1007/s43236-022-00491-1

[19] Heo, KW., Choi, HJ. & Jung, JH. Real-time test-bed system development using power hardware-in-the-loop (PHIL) simulation technique for reliability test of DC nano grid. J. Power Electron. 20, 784–793 (2020).https://doi.org/10.1007/s43236-020-00075-x.